Monthly Notices
of the
ROYAL ASTRONOMICAL SOCIETY

Mon. Not. R. Astron. Soc. **408,** 383–391 (2010) doi:10.1111/j.1365-2966.2010.17115.x

Discovery of the afterglow and host galaxy of the low-redshift short GRB 080905A⋆

A. Rowlinson,[1]† K. Wiersema,[1] A. J. Levan,[2] N. R. Tanvir,[1] P. T. O'Brien,[1] E. Rol,[3] J. Hjorth,[4] C. C. Thöne,[5] A. de Ugarte Postigo,[5] J. P. U. Fynbo,[4] P. Jakobsson,[6] C. Pagani[1,7] and M. Stamatikos[8,9]

[1]*Department of Physics & Astronomy, University of Leicester, University Road, Leicester LE1 7RH*
[2]*Department of Physics, University of Warwick, Coventry CV4 7AL*
[3]*Astronomical Institute 'Anton Pannekoek', University of Amsterdam, PO Box 94249, 1090 GE Amsterdam, the Netherlands*
[4]*Dark Cosmology Centre, Niels Bohr Institute, University of Copenhagen, Juliane Maries Vej 30, 2100 Copenhagen, Denmark*
[5]*Istituto Nazionale di Astrofisica, Osservatorio Astronomico di Brera, via E. Bianchi 46, I-23807 Merate, Italy*
[6]*Centre for Astrophysics and Cosmology, Science Institute, University of Iceland, Dunhagi 5, 107 Reykjavík, Iceland*
[7]*Department of Astronomy and Astrophysics, Pennsylvania State University, 525 Davey Laboratory, University Park, PA 16802, USA*
[8]*NASA Goddard Space Flight Center, Greenbelt, MD 20771, USA*
[9]*Center for Cosmology and Astro-Particle Physics (CCAPP) Fellow/Department of Physics, The Ohio State University, 191 West Woodruff Avenue, Columbus, OH 43210, USA*

Accepted 2010 May 30. Received 2010 May 5; in original form 2010 February 18

ABSTRACT

We present the discovery of short GRB 080905A, its optical afterglow and host galaxy. Initially discovered by *Swift*, our deep optical observations enabled the identification of a faint optical afterglow, and subsequently a face-on spiral host galaxy underlying the GRB position, with a chance alignment probability of <1 per cent. There is no supernova component present in the afterglow to deep limits. Spectroscopy of the galaxy provides a redshift of $z = 0.1218$, the lowest redshift yet observed for a short GRB. The GRB lies offset from the host galaxy centre by $\sim$18.5 kpc, in the northern spiral arm which exhibits an older stellar population than the southern arm. No emission lines are visible directly under the burst position, implying little ongoing star formation at the burst location. These properties would naturally be explained were the progenitor of GRB 080905A a compact binary merger.

Key words: gamma-ray burst: individual: GRB 080905A.

1 INTRODUCTION

The detection of the first fading afterglow from long gamma-ray bursts (LGRBs) (Costa et al. 1997; van Paradijs et al. 1997) proved to be a pivotal moment in their study. Similarly, the first identifications of short GRB (SGRB) afterglows in 2005 opened a new window on this still enigmatic class of transient (Gehrels et al. 2005; Hjorth et al. 2005; Fox et al. 2005; Berger et al. 2005). Afterglows provide precise positions, and hence a route to redshifts and identifying the host galaxies. This in turn provides luminosities and space densities for the bursts, allows possible means of measuring their collimation and ultimately may enable 'smoking' gun signatures of their progenitors to be uncovered, as was the case for LGRBs (Hjorth et al. 2003).

GRBs can be categorized, largely according to their duration, as LGRBs and SGRBs, with the dividing line being at roughly 2 s (Kouveliotou et al. 1993). LGRBs have been identified with star-forming galaxies with moderately low metallicity (e.g. Bloom, Kulkarni & Djorgovski 2002; Fruchter et al. 2006) leading to the suggestion that young massive stars are the most likely progenitors (collapsars; summarized in Woosley & Bloom 2006). Studies of the locations of LGRBs with the *Hubble Space Telescope* (*HST*) have shown that LGRBs typically occur in compact galaxies (Fruchter et al. 2006; Wainwright, Berger & Penprase 2007), with mean effective radii of 1.7 kpc, and in the brightest regions of their hosts (Bloom et al. 2002; Fruchter et al. 2006). However, studies of SGRB host galaxies contrast with this picture. Some hosts contain exclusively ancient populations (Berger et al. 2005; Gehrels et al. 2005; Bloom et al. 2006), while others are actively star forming (Fox et al. 2005; Levan et al. 2006), or contain a mixture of young and older populations (Soderberg et al. 2006). Additionally, the bursts themselves can be significantly offset from their hosts (Berger et al. 2005; Fox et al. 2005; Bloom et al. 2006; Troja et al. 2008), a fact which

⋆Based on observations at ESO telescopes at Paranal Observatory under programme ID 081.D-0588.
†E-mail: bar7@star.le.ac.uk

can complicate the task of host identification (Levan et al. 2007). These observations imply that the progenitors of SGRBs can originate from ancient populations, which may well be kicked from their birthplace. The final mergers of compact object binaries remain a prime candidate (Lattimer & Schramm 1976; Eichler et al. 1989; Narayan, Paczynski & Piran 1992). Additionally, there is thought to be a separate population of SGRBs at redshifts $\ll 0.1$ which are associated with giant flares from extra-galactic Soft Gamma Repeaters (Hurley et al. 2005; Tanvir et al. 2005). At very low redshift there may be overlap between these, and a more energetic, cosmological population.

With the influx of GRBs over the past few years, it has become apparent that there are examples of SGRBs and LGRBs which have properties which make it hard to unambiguously assign them to one category or the other. For example GRB 050724, $T_{90} = 3$ s, occurred in a nearby elliptical galaxy which, among other properties, associated it with the SGRB population (Barthelmy et al. 2005; Berger et al. 2005). GRB 060505, $T_{90} = 5$ s, had no associated supernova but had a spectral lag which is consistent with the LGRB population, was located within a star formation region in a host galaxy at $z = 0.09$ and its classification is still not firmly established (Fynbo et al. 2006; Ofek et al. 2007; Jakobsson & Fynbo 2007; Thöne et al. 2008; McBreen et al. 2008; Bloom, Butler & Perley 2008; Xu et al. 2009). Additionally, GRB 060614, $T_{90} = 100$ s, is thought to be a SGRB with extended emission as there was no associated supernova and the spectral lag was consistent with other SGRBs (Fynbo et al. 2006; Gal-Yam et al. 2006; Zhang et al. 2007). Recently, GRB 090426 was identified as the most distant SGRB at a redshift of $z = 2.609$ and $T_{90} = 1.28$ s (Levesque et al. 2010a; Thöne et al. in preparation). Levesque et al. (2010a) and Antonelli et al. (2009) conclude from their observations that the simplest explanation is that the progenitor was more likely to be a collapsar. With this in mind, it is imperative that we understand the properties of host galaxies and, if possible, the local environment of GRBs to aid in their classification and the identification of the progenitor.

The majority of GRBs lie at moderate to high redshift, and have host galaxies which are at best only marginally resolved from the ground. Most SGRB redshifts to date come from the putative host galaxy and in some cases these may be ambiguous (Levan et al. 2007). GRBs 060505 (Thöne et al. 2008), 020819 (Levesque et al. 2010b) and 980425 (Michałowski et al. 2009) have been identified in nearby host galaxies, which has allowed more detailed spectroscopy. Instead of relying on the properties of the galaxy as a whole, it has been possible to subdivide the galaxy into relevant regions and complete spatially resolved spectroscopy. This has allowed the study of the region in which the GRB occurred giving details about the local stellar population.

Here, we present the discovery of the optical afterglow, and host galaxy of the short GRB 080905A. Its faint afterglow pinpointed its location to a spiral host galaxy at $z = 0.1218$, the most local short burst yet known. SGRB 050709 has the next lowest confirmed redshift for a SGRB at $z = 0.16$ (Fox et al. 2005), followed by SGRB 050724 associated with a host galaxy at $z = 0.257$ (Barthelmy et al. 2005; Berger et al. 2005). SGRB 061201 may be associated with a galaxy at lower redshift of $z = 0.111$ but it was not possible to confirm this as it was offset by 17 arcsec (Stratta et al. 2007). In Section 2, we describe the observations obtained of the afterglow of GRB 080905A and the spectra obtained for the host galaxy. We analyse these data in Section 3, discuss the implications of our findings in Section 4 and draw our conclusions in Section 5.

Throughout the paper, we adopt a cosmology with $H_0 = 71\,\mathrm{km\,s^{-1}\,Mpc^{-1}}$, $\Omega_\mathrm{m} = 0.27$, $\Omega_\Lambda = 0.73$. A redshift of $z = 0.1218$ then gives a luminosity distance of 562.3 Mpc, and 1 arcsec corresponds to 2.17 kpc. The errors are quoted at 90 per cent confidence for X-ray and 1σ for optical.

2 OBSERVATIONS AND ANALYSIS

2.1 Prompt emission properties

GRB 080905A was detected by *Swift* at 11:58:54 UT. It is a SGRB with T_{90} duration of 1.0 ± 0.1 s; the Burst Alert Telescope (BAT) detected three flares peaking at $T + 0.04067 \pm 0.0007$ s, $T + 0.17^{+0.03}_{-0.10}$ s and $T + 0.869 \pm 0.003$ s. The time-averaged BAT spectrum was best fit by a power law with a photon index of $\Gamma = 0.85 \pm 0.24$ and the fluence was $(1.4 \pm 0.2) \times 10^{-7}$ erg cm^{-2} in the 15–150 keV energy band (Cummings et al. 2008). The flux at a specific frequency, ν, and time are given by $f_\nu \propto \nu^{-\beta} t^{-\alpha}$ where $\beta = \Gamma - 1$. GRB 080905A was also detected by *INTEGRAL* (Pagani & Racusin 2008) and *Fermi* Gamma-ray Burst Monitor (GBM) (Bissaldi et al. 2008). Using the redshift of 0.1218, the isotropic energy released is $4.7 \pm 0.7 \times 10^{49}$ erg in the 15–150 keV energy band.

Some short GRBs show evidence for a soft extended emission component in the prompt emission (e.g. Barthelmy et al. 2005; Norris & Bonnell 2006). There is no evidence of soft extended emission in the BAT 15-25 keV light curve for GRB 080905A, with a limiting flux of $<5.2 \times 10^{-7}$ erg cm^{-2} s^{-1}.

Additionally, short GRBs have negligible spectral lag in their prompt emission unlike long GRBs (Norris & Bonnell 2006; Yi et al. 2006). We performed a spectral lag analysis of GRB 080905A based on the cross-correlation function methodology used in Ukwatta et al. (2010). The analysis considered several time-scales using 128, 64, 32, 16, 8 and 4 ms binned light curves and compared all six pairing combinations of the BAT 's four energy channels. There is a lack of emission below 25 keV, which results in very low cross-correlation amplitudes for paired light curves containing channel 1. Channels 2 and 4 also have relatively low emission, so in this analysis we use cross-correlation between channels 2 and 3 and determine the lag using a Gaussian fit. We calculate the 1σ error using 1000 lag Monte Carlo simulations. The lag time of GRB 080905A is 4 ± 17 ms, which is consistent with zero as expected for a short GRB.

2.2 X-ray afterglow observations

The fading X-ray afterglow was located by *Swift* with an enhanced position of RA (J2000): 19 10 41.74 and Dec. (J2000): −18 52 48.8 with an uncertainty of 1.6 arcsec (90 per cent confidence) (Evans, Osborne & Goad 2008).

The time-averaged X-ray Telescope (XRT) spectrum using the photon counting (PC) data is best fit by an absorbed power law with photon index $\Gamma = 1.45 \pm 0.25$ and with an intrinsic absorption $N_\mathrm{H} = 1.6 \pm 1.0 \times 10^{21}$ cm^{-2} in excess of the Galactic absorption of $N_\mathrm{H} = 9 \times 10^{20}$ cm^{-2} (Kalberla et al. 2005). We fit the combined BAT/XRT light curve with power-law decay models with one break. The best-fitting spectrum is $\alpha_1 = 2.62^{+0.25}_{-0.13}$, breaking at $T_1 = 443^{+408}_{-84}$ s to a decay of $\alpha_2 = 1.49^{+0.60}_{-3.66}$. The BAT count rates (in the 15–150 keV energy band) were extrapolated to the XRT energy band (0.3–10 keV) and converted to flux using the average spectral index for the BAT and XRT PC spectra and standard tasks in XSPEC. These fluxes were then combined with the XRT light curve to create the combined BAT/XRT light curve. Using the redshift of 0.1218 and a k-correction (Bloom, Frail & Sari 2001), the combined

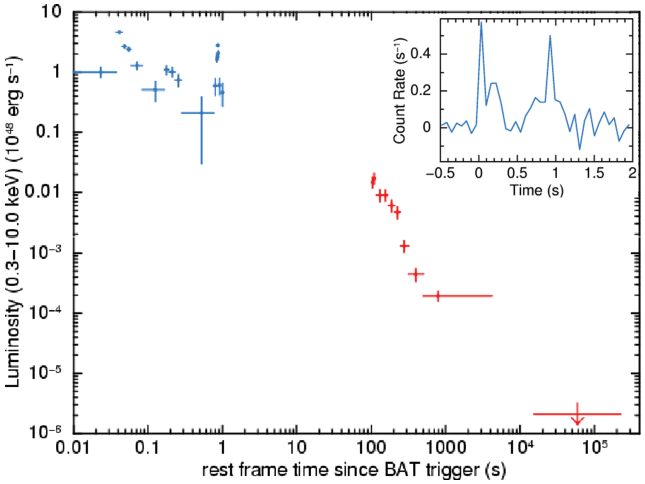

Figure 1. This shows the combined BAT and XRT luminosity and rest-frame light curve for GRB 080905A. The BAT data are plotted until ∼2 s and the XRT data are plotted starting at ∼100 s. Inset is the BAT light curve with linear observed time on the horizontal axis and BAT count rate on the vertical axis.

BAT/XRT light curve has been converted to the rest-frame time and luminosity and is shown in Fig. 1.

2.3 Optical observations

Early optical imaging of GRB 080905A obtained only upper limits on the afterglow flux, which were found by UVOT at $T+114$ s (V > 21.3; Brown & Pagani 2008), the Mt. John Observatory at $T+2580$ s (R > 20.8; Tristram et al. 2008) and the MITSuME telescope at $T+2520$ s (R > 17.6) (Nakajima et al. 2008).

Our observations began at the Nordic Optical Telescope (NOT) 8.5 h after the burst, with further epochs obtained with the Very Large Telescope (VLT) utilizing FORS2 taking place 14.3 and 36 h after the burst. A final *R*-band observation was made on September 23, 17.5 days post burst. Using ISAAC, we obtained a further *K*-band observation on October 1, 25.5 d post burst. Comparison of these observations allowed us to discover both a faint optical afterglow and an underlying spiral host galaxy (Malesani et al. 2008; de Ugarte Postigo et al. 2008).

Our optical images were reduced in the standard fashion, and magnitudes for the afterglow derived in comparison to USNO and Two-Micron All Sky Survey (2MASS) objects within the field (since conditions were not photometric at the time of the observations). As the afterglow lies on the edge of its spiral host we obtain host-subtracted afterglow fluxes by subtraction of the light from this galaxy, assuming zero contribution of transient light in the final epoch of optical images. The resulting magnitudes are shown in Table 1. The afterglow is faint $R \sim 24$, even for a SGRB, and demonstrates the necessity of deep and rapid observations in the location of SGRBs. Converting the optical magnitude of GRB 080905A to a flux of $\sim 7 \times 10^{-30}$ erg cm^{-2} s^{-1} Hz^{-1} and comparing it to the sample at 11 h considered by Nysewander, Fruchter & Pe'er (2009), it is one of the faintest afterglows detected and, with a optical luminosity of $\sim 6.7 \times 10^{25}$ erg s^{-1} Hz^{-1}, the lowest luminosity optical afterglow detected and lies below the trend observed between optical afterglow intensity and isotropic energy, suggesting that this GRB occurred in a low-density environment. We used a reasonable extrapolation of the X-ray light curve to the time of our optical imaging to determine that the non-detection of the X-ray afterglow is consistent with the decay observed. The location of the optical afterglow is RA (J2000): 19 10 41.71 and Dec. (J2000): −18 52 47.62, with an error of 0.76 arcsec, and is shown in Fig. 2.

The afterglow is located ∼9 arcsec from the centre of an $R \sim 18$ galaxy, and we conclude that this is the host galaxy. To calculate the likelihood of a chance alignment of a similar or brighter galaxy within 10 arcsec of the afterglow we use the host galaxy magnitude and size and the number of galaxies of this magnitude or brighter (Hogg et al. 1997). The probability of a chance alignment is less than 1 per cent. A more accurate method would be to use the half light radius of the galaxy as described in Fong, Berger & Fox (2010); however it is difficult to calculate this due to contamination of foreground stars. The low chance probability and the fact that the afterglow location lies within the stellar field of the galaxy both support our conclusion that this is the host galaxy of GRB 080905A. As for many GRBs without afterglow redshifts, it is possible that GRB 080905A is associated with a higher redshift galaxy which is fainter than the deep limiting magnitude of our optical images ($R > 25$).

The location of the afterglow is offset from the centre of the host galaxy by a projected radial distance of 18.5 kpc. This is a relatively large offset, but is comparable to several other SGRB locations (Troja et al. 2008; Fong et al. 2010) and it is important to note that the host galaxy is relatively large so the host-normalized offset would be much smaller. Host-normalized offsets are calculated by normalizing the offset to the effective (half light) radius of the host galaxy.

At a redshift of $z = 0.1218$ a supernova like SN 1998bw would reach a peak magnitude of roughly $R \sim 19.5$, a factor of >100 brighter than any object present in our final epoch. The lack of any visible supernova component is in keeping with searches which have done in other SGRBs, supporting our classification of GRB 080905A as a member of the SGRB population. For example, Hjorth

Table 1. Log of observations of the afterglow and host of GRB 080905A. The magnitudes shown for the afterglow are host subtracted, assuming zero contamination from the afterglow in epoch 4. Magnitudes have been corrected for foreground extinction of $E(B-V) = 0.14$.

Epoch	Date midpoint (UT)	Start time after trigger (h)	Telescope	Exposure time (s)	Filter/grism	Seeing (arcsec)	Magnitude
1	Sept 05 20:30 UT	8.5	NOT	1800	*R*	0.9	24.04 ± 0.47
2	Sept 06 02:39 UT	14.3	VLT	2400	*R* special	1.05	24.26 ± 0.31
3	Sept 07 00:29 UT	36	VLT	2400	*R* special	0.85	>25.0
4	Sept 23 00:44 UT	-	VLT	2400	*R* special	0.85	-
5	Oct 01 01:15 UT	-	VLT	7200	*K* short	0.65	-
(Slit position 1)	Sept 24 01:39 UT	-	VLT	3600	Grism	0.9	-
(Slit position 2)	Sept 24 02:27 UT	-	VLT	3600	Grism	0.9	-

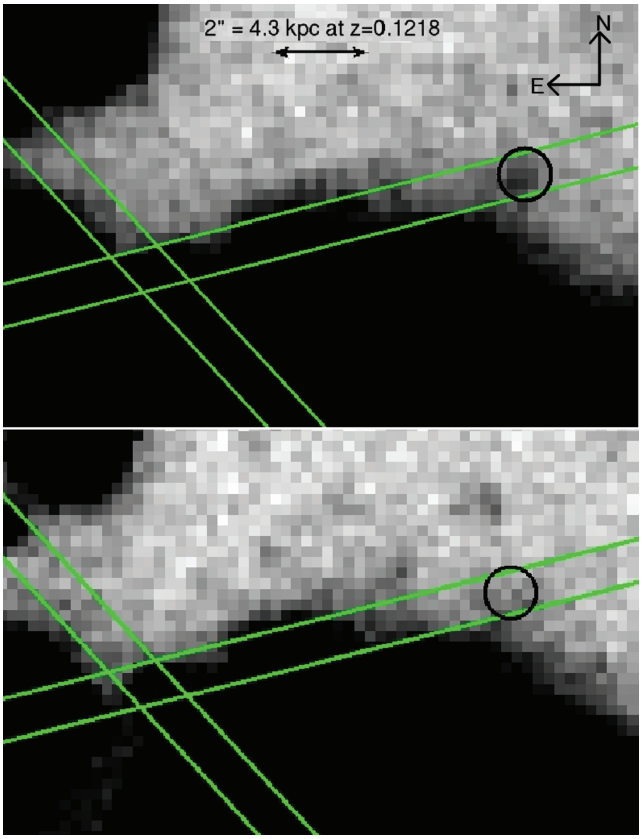

Figure 2. The circle marks the location of the afterglow of GRB 080905A, the top image is from epoch 2, observed 14.3 h after the trigger time, and the bottom image is from epoch 4, ∼18 d after the trigger time (see Table 1). For reference, the two slit positions used for spectroscopy have also been included.

et al. (2005) conducted an early search for an SN component for SGRB 050509B finding any accompanying SN would be fainter than typical SNe and Fox et al. (2005) conducted place deep limits for an SN component for SGRB 050709. Our observations can also be used to probe the possible production of radioactive nickel during GRB 080905A. The ejection of radioactive material in the process of an NS–NS merger may create a visible electromagnetic signal described as a mini-SN (Li & Paczyński 1998; Kulkarni 2005; Metzger, Piro & Quataert 2008; Kocevski et al. 2010). The absence of any late time emission brighter than $R \sim 24$ coupled with the known low redshift makes these constraints strong in the case of GRB 080905A, although the cadence of the observations is sensitive to either relatively fast or slow rise time (but not those of intermediate duration). This suggests that the radioactive yield associated with GRB 080905A is $<0.01\ M_{\odot}$, based on the low-redshift model developed by Perley et al. (2009) for GRB 080503 and the general models in Kulkarni (2005).

2.4 Host galaxy spectroscopy

To characterize the host galaxy, we obtained deep spectroscopy on 2008 September 24, using FORS1 on UT2 of the VLT, Chile. These observations were obtained after the optical afterglow had faded. To maximize wavelength coverage we used the 300 V grism with the GG375 filter to suppress contamination by the second spectral order. This results in a wavelength range ∼3700 to 9200 Å.

The 1.0 arcsec wide slit was oriented along two different fixed position angles, illustrated in Fig. 3, and 4 × 450 s exposures were

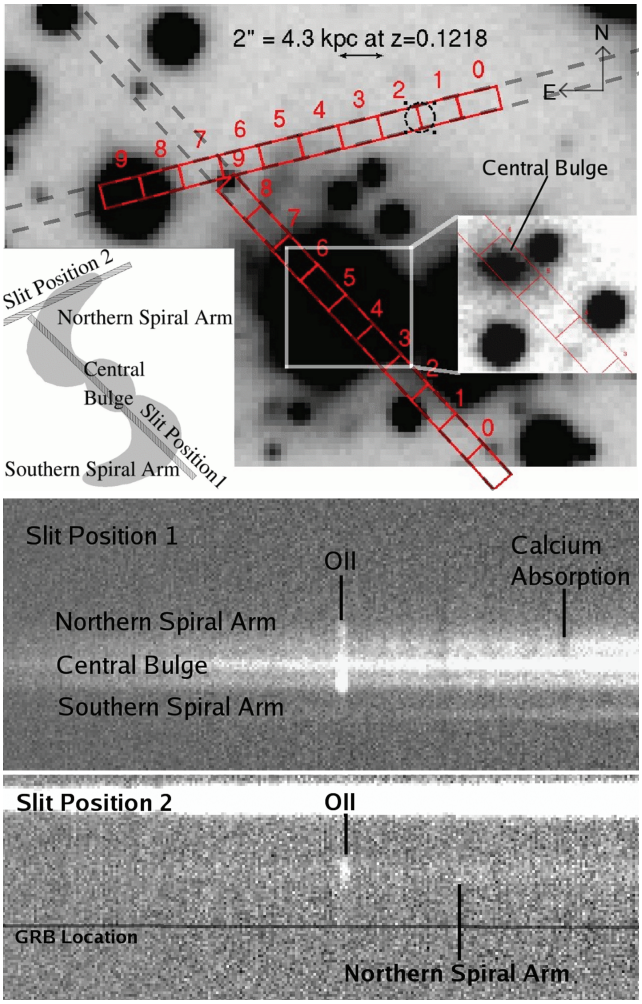

Figure 3. This shows the locations of the two slit positions used to obtain the spectra (dashed lines) and the subapertures into which the spectra were divided into subspectra. The dashed circle shows the location of the optical afterglow. The main image shows the spiral arms in the *R* band. The inset on the right shows the central bulge of the galaxy in the *K* band. In the bottom left corner, there is a sketch of the structure of the galaxy. In the middle panel, the 2D spectra are there for slit position 1 in which the emission lines get fainter when moving from the southern spiral arm to the northern spiral arm and the absorption features dominate more in the northern spiral arm than in the southern spiral arm. Additionally, the continuum in the northern spiral arm is fainter than the southern spiral arm bluewards of the D4000 break. In the bottom panel is the 2D spectra for slit position 2 in which faint emission lines can be observed and the continuum of the northern spiral arm. The horizontal line shows the location of the GRB.

acquired for each slit position. The two slit positions (−104.°1 and −42.°7) were chosen to cut through the host galaxy covering the nucleus as well as spiral arms on either side of the galaxy (hereafter 'slit position 1'), and to cover the afterglow position and cut through a nearby spiral arm (hereafter 'slit position 2'). Seeing conditions during the observations were reasonable with an average seeing of 0.9 arcsec and mean airmass of 1.2 (slit position 1) and 1.3 (slit position 2). We reduced the data using standard procedures in IRAF. The four exposures per slit position were combined before extraction, removing cosmic rays in the process.

We extracted the spectra of slit position 1 and 2 in the same way: we use the relatively bright continuum of the bulge (slit position 1) or a nearby bright star (slit position 2) to fit the shape of the trace

function, and extract using 10 adjoining, equally sized subapertures following this trace. Subapertures are 7 pixels in size in both slit position 1 and 2 data, which corresponds to 1.76 arcsec per subaperture (pixel scale is 0.252 arcsec per pixel), i.e. a value matched to twice the seeing full width at half-maximum (FWHM). At the redshift of the host galaxy, this corresponds to a physical scale of 3.8 kpc per subaperture. In the following we will refer to the spectra extracted with these small apertures as subspectra. Fig. 4 shows examples of extracted subspectra. The GRB location is covered only by slit position 2, and falls in subapertures 1 and 2. The subspectra are wavelength calibrated using He, HgCd and Ar lamp spectra. From the FWHM of a Gaussian fit on the arc lines we measure a nominal spectral resolution of 11 Å at the central wavelength.

Flux calibration of the subspectra was done using observations of the spectrophotometric standard star LDS 749B. Atmospheric extinction correction was done by applying the average Cerro Tololo Inter-American Observatory (CTIO) atmospheric extinction curve. A Galactic dust extinction correction was performed by using the $E(B-V)$ value of 0.14 (Schlegel, Finkbeiner & Davis 1998), and assuming a Galactic extinction law A_λ/A_V expressed as $R_V = A_V/E(B-V)$ (Cardelli, Clayton & Mathis 1989). We make the standard assumption $R_V = 3.1$ (Rieke & Lebofsky 1985). No Galactic Na I or K I absorption is detected in the spectrum, consistent with the $E(B-V)$ value from Schlegel et al. (1998). Note that this calibration provides us with a good *relative* flux calibration needed to evaluate changes between the different subspectra, e.g. in the strength of emission line ratios or some continuum features, but does not provide a full absolute calibration.

From the detected emission lines we measure the redshift of the GRB host galaxy to be $z = 0.1218 \pm 0.0003$.

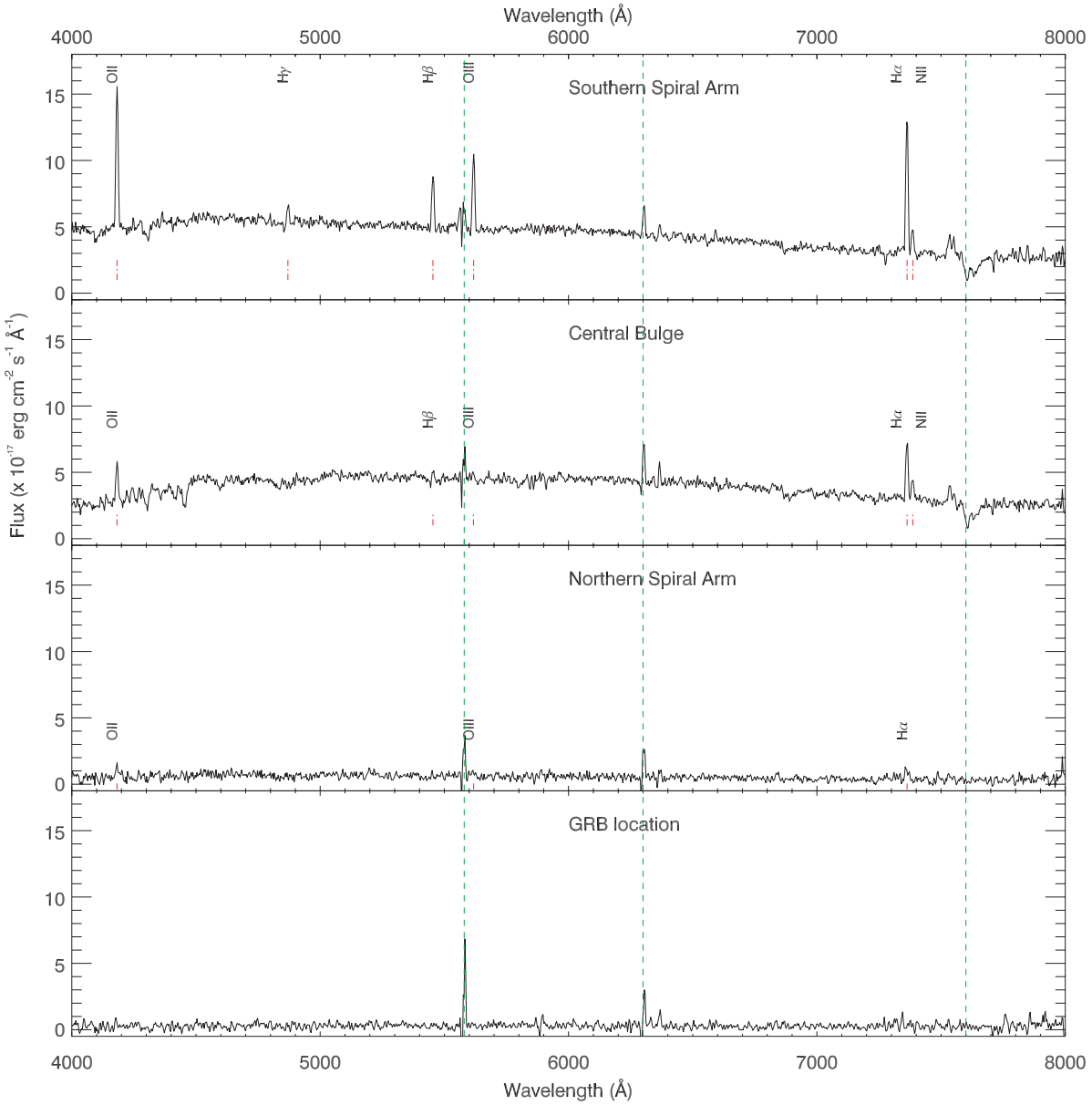

Figure 4. This shows the observed spectra in the northern spiral arm, the central bulge and the southern spiral arm. These correspond to subapertures 4, 6 and 8 from slit position 1. The lowest panel shows the observed spectrum at the GRB location. There are residual features from sky line subtraction at ∼5600 Å, ∼6300 Å and ∼7600 Å (shown by the dashed lines).

3 HOST GALAXY PROPERTIES

3.1 Host morphology

Visual inspection of the images in *R* and *K* bands shows the host to be a nearly face-on galaxy, with clear bulge, disc and spiral arm components. At least two spiral arms can be distinguished, one on either side of the galaxy, which are hard to see due to a great number of foreground stars. Fig. 3 shows the spiral arms as observed in the *R* band and inset is an image of the central bulge in the *K* band. The detection of spiral arms in combination with the detected emission and absorption lines allows us to loosely classify the host of GRB 080905A as an Sb/c galaxy.

By subtracting foreground stars from the images we estimate that the host of GRB 080905A has an *R*-band magnitude of $R = 18.0 \pm 0.5$. The large error arises not due to the faintness of the object, but due to the uncertainty in subtracting the significant number of foreground sources which overlap the spiral structure. Correcting for foreground extinction [$E(B-V) = 0.14$] this corresponds to an absolute magnitude of $M_V \sim -21$, and suggests that the host of GRB 080905A is broadly similar to the Milky Way.

Using the near-infrared mass–light ratio, $M_{*,\rm old}(\rm M_\odot) = 2.6 \times 10^8 D^2(\rm Mpc) F_k(\rm Jy)$ (Thronson & Greenhouse 1988), and the *K*-band magnitude of the host galaxy, $K = 16.2^{+0.4}_{-0.7}$, we determine the mass of the host galaxy to be $M_{*,\rm old} = 2 \pm 1 \times 10^{10}\,\rm M_\odot$. The errors are estimated based on the uncertainties in subtraction of the foreground stars and identifying the extent of the host galaxy.

3.2 Rotation curve

The nearly face-on orientation of the host galaxy gives us an excellent view of the location of the GRB within the host, similar to GRB 060505 which also occurred in nearly face-on Sbc galaxy (Thöne et al. 2008). However, this favourable geometry complicates the measurements of the host dynamical mass, required to test the consistency of this host, and GRB spiral hosts in general, with the mass–metallicity relation at this redshift.

Visual inspection of the 2D spectrum shows no clear slant in the [S II], Hα, [N II], [O III], Hβ and [O II] lines ([O II] are shown in Fig. 4). To determine the rotation curve of the galaxy (or upper limits) we use the FXCOR routines in the IRAF RV package to Fourier cross-correlate the spectra of different subapertures of the slit position 1 spectra, finding their relative radial velocity as a function of distance to the galactic nucleus. We correlate spectral sections around the brightest emission lines, as well as the full subaperture spectra (using also absorption features). We fit a Gaussian function to the cross-correlation peak to determine its centre and width. Between the two subspectra with the highest signal-to-noise ratio emission lines, subapertures 3 and 7, we find a formal radial velocity difference of $19 \pm 38\ \rm km\,s^{-1}$. Using symmetrical subapertures about the Galactic Centre (4 and 8) we find $30 \pm 160\ \rm km\,s^{-1}$. This value is using very weak emission lines in subaperture 8, so is a much less constraining limit.

Using the GALFIT software package (Peng et al. 2002), we decompose the host galaxy to identify the inclination angle. We use the acquisition images for the spectra, which have the best seeing conditions. We use an empirical point spread function (PSF) as modelled through the IRAF DAOPHOT routines using several moderately bright stars close to the GRB position. We find an inclination angle of $\sim 23^\circ$; however there are large errors associated with this value due to poor signal-to-noise ratio, contamination by bright stars and the near face-on inclination. This angle appears to be smaller than that identified for LGRB 980425, $\sim 50^\circ$ (Christensen et al. 2008).

3.3 Spatially resolved properties

The middle and bottom panels of Fig. 3 show the subspectra from slit position 1 and 2, in which differences in continuum shape and line properties can be seen, reflecting subtle changes in stellar population properties dominating the differing subspectra. From Fig. 3, it is clear that several field stars are located close to and on top of the host. Some of the subspectra appear affected by light from these stars, which can be seen by the presence of Balmer, Na and Ca lines at zero redshift, and from the shape of the continuum.

The 2D spectra clearly show several basic properties of the host. In Fig. 4, we show subspectra from subapertures 4 (northern spiral arm), 6 (central bulge) and 8 (southern spiral arm) from slit position 1. Additionally, we show the subspectra from subaperture 2 for slit position 2, corresponding to the GRB location. The slit position 1 spectrum shows that the nebular emission lines are strongest in the southern part of the host, and get dramatically weaker northwards of the nucleus. This shows that the star formation rate is strongest in the spiral arm diametrically opposite the GRB position, in stark contrast to the spiral host galaxy of LGRBs 980425, that show strongest star formation at, or near, the location of the burst (Christensen et al. 2008). The GRB location appears to lie in the extension of a spiral arm. The 2D spectrum of slit position 2, which probes this arm, clearly shows strong nebular emission lines of [O III] and [O II], and weaker Hα and Hβ at the location of the spiral arm, but no emission line flux is detected at the location of the burst. At and near the GRB location, a weak, near featureless continuum can be seen.

The slit position 1 subspectra that are dominated by bulge light show clear absorption features common to old populations and interstellar medium (ISM) gas (Na I, Ca II, 4000 Å break, *G* band), and show stellar atmosphere Balmer absorption underneath the nebular Balmer emission. The other spectra have brighter nebular lines and weaker 4000 Å breaks. As several of the subspectra are contaminated by light from foreground stars, and the resolution of the spectra is low, we limit our analysis in this paper to the nebular emission lines and the strongest absorption bands.

Using the relative fluxes of Hα and Hβ, we are able to determine the flux ratio at different points in the host galaxy, as shown in Fig. 5. This gives an indication of the reddening in the host galaxy, which is important to consider as the metallicities and D4000 we calculate may be affected by this value. Fig. 5 shows that the southern spiral arm and central bulge are consistent with having little significant reddening. However, the northern spiral arm shows significant reddening, and this will affect our R23 calculations.

We measure the emission line fluxes in each subspectrum in slit position 1, and compute the metallicity profile along this slit position through the *N*2 indices, where $N2 \equiv [\rm N_{II}]\lambda 6583/\rm H\alpha$ (Pettini & Pagel 2004). In addition to these indices, we compute R23 metallicities where possible using $R23 \equiv ([\rm O_{II}] + [\rm O_{III}])/\rm H\beta$ (Pettini & Pagel 2004).

In the slit position 2 subspectra we can only determine emission line upper limits at the GRB location. The metallicity of the spiral arm that is covered by slit position 2 can be calculated through R23.

In Fig. 5, we show the log(N2) index (also converted into 12+log(O/H), calibrated using nearby extragalactic H II regions, as defined by Pettini & Pagel 2004), the Hα flux and R23 metallicity as a function of distance in kpc from the centre of the galaxy (the centre is taken to be the centre of subaperture 6). In the three horizontal panels we provide these values for slit position 1, slit position

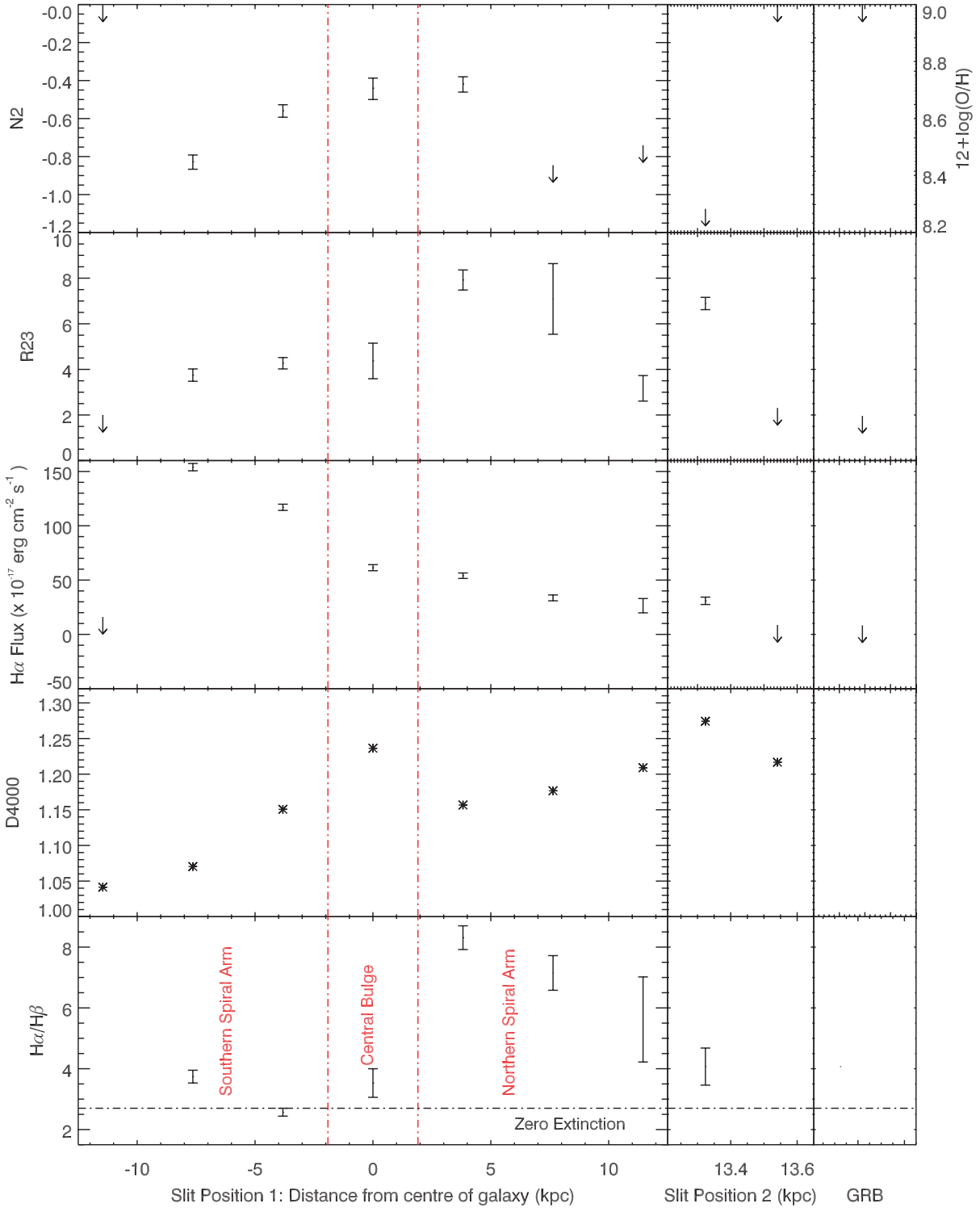

Figure 5. Panel 1 shows the Log(N2), Hα flux, R23, D4000 and the flux ratio of Hα to Hβ as a function of position from the centre of the host galaxy. Note that the Hα flux can only be used as a relative value as it has not been absolutely calibrated. In the lowest panels, we show the Hα to Hβ ratio for zero extinction. In the second panel is the data from slit position 2 along the spiral arm and the third shows the upper limits for the region in which the GRB occurred.

2 (for the spiral arm in subapertures 4 and 5, subaperture 6 is contaminated by a nearby star) and near the GRB location (subaperture 1). The log(N2) index, where it was possible to measure, shows an increasing metallicity from the southern spiral arm, through the central bulge and into the northern spiral arm. The 12+log(O/H) value increases from 8.4 in the southern spiral arm to 8.7 in the northern spiral arm. This is reinforced by the findings for R23 metallicity, which also shows that the northern spiral arm has a higher metallicity than the central bulge and southern spiral arm. We convert the R23 metallicity into 12+log(O/H) using the KK04 method in Kewley & Ellison (2008) and break the degeneracy between the two solutions using the result for log(N2). The errors on these values

can be estimated from the errors on the R23 values shown in Fig. 5; however there is an uncertainty associated with using the KK04 method in Kewley & Ellison (2008) which is difficult to quantify. We find the metallicity at 2 kpc from the centre of the host to be 8.9 or 8.1 in the southern spiral arm (it was not possible to break the degeneracy between the two solutions in this arm), 8.9 in the central bulge, 8.5 in the northern spiral arm and 8.5 in slit position 2 at 13.4 kpc from the centre of the galaxy. However, these values for metallicity calculated using R23 are likely to be affected by reddening in the host galaxy and the 12+log(O/H) metallicity is reliant on breaking the degeneracy of two solutions. Therefore, we base our analysis on the values obtained using log(N2) where possible and use the R23 values to corroborate the general result. The values obtained for log(N2) are less sensitive to reddening due to the close proximity of the two lines used to calculate this value. Taking the solar metallicity to be 8.69 (Asplund et al. 2004), we note that the southern spiral arm has 0.5 $Z_{\odot}$ and the central bulge and northern spiral arms have a value of 1 $Z_{\odot}$. In the southern spiral arm, we can infer a metallicity gradient of -0.07 dex kpc^{-1}, which is consistent with the Milky Way gradient of -0.09 ± 0.01 dex kpc^{-1} (Smartt & Rolleston 1997; Rolleston et al. 2000). The Hα flux shows a decreasing trend from the southern spiral arm to the northern spiral arm. The results from the spiral arm in slit position 2 tend to be in agreement with the northern spiral arm in slit position 1. These results show that the southern spiral arm is an actively star-forming region and this is in direct contrast to the northern spiral arm. The limits at the GRB location are provided for reference. The GRB is in the northern spiral arm, on the opposite side of the galaxy to the active star formation.

In addition to the emission line properties, we measure the 4000 Å break (D4000), which is a useful diagnostic for age and metallicity which can even be measured in relatively low signal-to-noise ratio (sub)spectra. Shortwards of 4000 Å is the start of stellar photospheric opacity, which takes into account the mean temperature of the stars. Hotter stars (with shorter lifetimes) have more ionized metals in their atmospheres, and hence a lower opacity, than cooler stars. This means that an older population of stars will have a higher opacity and, subsequently, a larger 4000 Å break (Bruzual 1983; Poggianti & Barbaro 1997; Gorgas et al. 1999; Kauffmann et al. 2003; Marcillac et al. 2006). Marcillac et al. (2006) have shown that D4000 is sensitive to metallicity once the age of the population exceeds a few billion years or when it is >1.6. D4000 is calculated using the ratio between two bands of the continuum, one redwards of the 4000 Å break and the other bluewards. We use the Balogh et al. (1999) definition of the D4000 continua, which is less wide than the original definition by Bruzual (1983), and therefore less affected by dust reddening. The calculated values are plotted in Fig. 5 and provide a qualitative estimate of the relative ages of the stars as a function of position in the galaxy. The estimated error for D4000 (calculated using the rms of the spectrum and the size of the bands) for slit position 1 is $\pm$0.12 and for slit position 2 is $\pm$0.65. As expected, it shows that the Galactic Centre hosts an older population of stars than the spiral arms. Interestingly, it also appears that the northern spiral arm hosts an older population of stars than the southern spiral arm. This reinforces the evidence of active star formation occurring within the southern spiral arm and not in the northern spiral arm. Due to large errors, it was not possible to calculate D4000 at the GRB location.

Using the approximate metallicity of this galaxy, log(O/H) + 12 $\sim$ 8.6 from log(N2), and the mass–metallicity relation as measured by Kewley & Ellison (2008) using galaxies in the Sloan Digital Sky Survey, we can estimate the mass of the galaxy to be $\sim 10^{10}$ $M_{\odot}$. This is consistent with the value calculated using the near-infrared mass–light ratio.

4 DISCUSSION

In the previous spatially resolved studies of low-redshift GRB host galaxies, it has been determined that LGRBs are associated with regions of active star formation and hence provide support for the core-collapse supernova progenitor theory, for example LGRB 980425 and LGRB 060218 (Fynbo et al. 2000; Wiersema et al. 2007; Christensen et al. 2008). Additionally, LGRBs at higher redshifts tend to occur in the brightest regions of the host galaxy (Fruchter et al. 2006; Svensson et al. 2010) and relatively small host galaxies (Wainwright et al. 2007). GRB 080905A is in direct contrast to these results, occurring on the opposite side of a relatively large spiral galaxy to the most active star formation region and significantly offset from the centre, so its progenitor is unlikely to be a massive star. The properties of this specific region of the host galaxy are in agreement with the findings of Prochaska et al. (2006) for typical SGRB environments. One of the theoretically predicted progenitors of SGRBs is the merger of a compact binary, for example two neutron stars or a neutron star and a black hole. Compact binaries are expected to be given a kick velocity during their formation which can allow them to travel large distances from their birthplace (Wang, Lai & Han 2006, and references therein). These events are expected to be associated with an older stellar population and offset from the host galaxy, as observed for GRB 080905A.

To summarize, GRB 080905A has short, hard prompt emission with properties expected for a compact binary merger progenitor. There was no associated supernova; it appears to be a low-density environment and had a low luminosity. The host galaxy is a spiral galaxy with active star formation, but GRB 080905A occurred close to a spiral arm, dominated by a relatively old population, and on the opposite side of the galaxy from the spiral arm with most active star formation. Additionally, it was offset from the centre of the host galaxy by a projected radial distance of 18.5 kpc. Therefore, our observations have shown that GRB 080905A is unambiguously a short-population GRB, whose properties suggest that the progenitor is likely to be a compact binary merger.

5 CONCLUSIONS

In this paper, we have presented spatially resolved spectroscopy of the host galaxy of the short hard GRB 080905A, with a T_{90} of 1 s. The prompt emission had an isotropic total energy of $\sim 5 \times 10^{49}$ erg in the energy band 15–150 keV. The X-ray and optical afterglows were observed, and the optical afterglow had a magnitude of $\sim$24 at 8.5 h after the burst fading to >25 at 32 h.

The host is an almost face-on spiral galaxy (inclination $\sim 23^{\circ}$) with a central bulge and at least two spiral arms; it is loosely classified as an Sb/c galaxy. The probability that GRB 080905A was chance aligned with this galaxy is <1 per cent. The observed redshift of this galaxy is $z = 0.1218 \pm 0.0003$, the lowest definite redshift for a typical SGRB thought to originate from a compact binary merger. Using spatially resolved spectroscopy, we identify a disparity between the two spiral arms, with the southern arm showing a younger stellar population and more active star formation than the northern spiral arm. We are unable to be more specific as we are using a relative flux calibration, not absolute fluxes, due to the contamination from overlying stars, and we are not observing the entire host galaxy.

The optical afterglow is observed to be offset from the centre of the galaxy by the projected radial distance of 18.5 kpc and occurs in the northern region. This offset and the association with an older population in the northern spiral arm, in addition to the prompt emission properties, shows that GRB 080905A would fit in the type I Gold sample GRB as defined by Zhang et al. (2009) with the progenitor being a compact binary merger.

ACKNOWLEDGMENTS

AR, KW, AJL and NRT would like to acknowledge funding from the Science and Technology Funding Council. PJ acknowledges support by a Marie Curie European Re-integration Grant within the 7th European Community Framework Programme under contract number PERG03-GA-2008-226653, and a Grant of Excellence from the Icelandic Research Fund. The Dark Cosmology Centre is funded by the DNRF. The financial support of the British Council and Platform Beta Techniek through the Partnership Programme in Science (PPS WS 005) is gratefully acknowledged. We thank A. Van Der Horst, B. Paciesas and T. Sakamoto for their help.

This work makes use of data supplied by the UK *Swift* Science Data Centre at the University of Leicester funded by the Science and Technology Funding Council. Based on observations made with the NOT, operated on the island of La Palma jointly by Denmark, Finland, Iceland, Norway and Sweden, in the Spanish Observatorio del Roque de los Muchachos of the Instituto de Astrofisica de Canarias. This research has made use of data obtained from the High Energy Astrophysics Science Archive Research Center (HEASARC), provided by NASA's Goddard Space Flight Center.

REFERENCES

Antonelli L. A. et al., 2009, A&A, 507, L45
Asplund M., Grevesse N., Sauval A. J., Allende Prieto C., Kiselman D., 2004, A&A, 417, 751
Balogh M. L., Morris S. L., Yee H. K. C., Carlberg R. G., Ellington E., 1999, ApJ, 527, 54
Barthelmy S. D. et al., 2005, Nat, 438, 994
Berger E. et al., 2005, Nat, 438, 988
Bissaldi E., McBreen S., Connaughton V., von Kienlin A., 2008, GCN, 8204, 1
Bloom J. S., Frail D. A., Sari R., 2001, AJ, 121, 2879
Bloom J. S., Kulkarni S. R., Djorgovski S. G., 2002, AJ, 123, 1111
Bloom J. S. et al., 2006, ApJ, 638, 354
Bloom J. S., Butler N. R., Perley D. A., 2008, AIPC, 1000, 11
Brown P. J., Pagani C., 2008, GCN, 8208, 1
Bruzual A. G., 1983, ApJ, 273, 105
Cardelli J. A., Clayton G. C., Mathis J. S., 1989, ApJ, 345, 245
Christensen L., Vreeswijk P. M., Sollerman J., Thöne C. C., Le Floc'h E., Wiersema K., 2008, A&A, 490, 45
Costa E. et al., 1997, Nat, 387, 783
Cummings J. et al., 2008, GCN, 8187, 1
de Ugarte Postigo A., Malesani D., Levan A. J., Hjorth J., Tanvir N. R., 2008, GCN, 8195, 1
Eichler D., Livio M., Piran T., Schramm D. N., 1989, Nat, 340, 126
Evans P. A., Osborne J. P., Goad M. R., 2008, GCN, 8203, 1
Fong W.-f., Berger E., Fox D. B., 2010, ApJ, 708, 9
Fox D. B. et al., 2005, Nat, 437, 845
Fruchter A. S. et al., 2006, Nat, 441, 463
Fynbo J. P. U., et al., 2000, ApJ, 542, L89
Fynbo J. P. U. et al., 2006, Nat, 444, 1047
Gal-Yam A. et al., 2006, Nat, 444, 1053
Gehrels N. et al., 2005, Nat, 437, 851
Gorgas J., Cardiel N., Pedraz S., González J. J., 1999, A&AS, 139, 29
Hjorth J. et al., 2003, Nat, 423, 847
Hjorth J. et al., 2005, ApJ, 630, L117
Hogg D. W., Pahre M. A., McCarthy J. K., Cohen J. G., Blandford R., Smail I., Soifer B. T., 1997, MNRAS, 288, 404
Hurley K. et al., 2005, Nat, 434, 1098
Jakobsson P., Fynbo J. P. U., 2007, preprint (arXiv:0704.1421)
Kalberla P. M. W., Burton W. B., Hartmann D., Arnal E. M., Bajaja E., Morras R., P öppel W. G. L., 2005, A&A, 440, 775
Kauffmann G. et al., 2003, MNRAS, 341, 33
Kewley L. J., Ellison S. L., 2008, ApJ, 681, 1183
Kocevski D. et al., 2010, MNRAS, 404, 963
Kouveliotou C. et al., 1993, ApJ, 413, L101
Kulkarni S. R., 2005, preprint (arXiv:astro-ph/0510256)
Lattimer J. M., Schramm D. N., 1976, ApJ, 210, 549
Levan A. J. et al., 2006, ApJ, 648, L9
Levan A. J. et al., 2007 MNRAS, 378, L1439
Levesque E. M. et al., 2010a, MNRAS, 401, 963
Levesque E. M., Kewley L. J., Graham J. F., Fruchter A. S., 2010b, ApJ, 712, L26
Li L.-X., Paczyński B., 1998, ApJ, 507, L59
Malesani D. et al., 2008, GCN, 8190, 1
Marcillac D., Elbaz D., Charlot S., Liang Y. C., Hammer F., Flores H., Cesarsky C., Pasquali A., 2006, A&A, 458, 369
McBreen S. et al., 2008, ApJ, 677, L85
Metzger B. D., Piro A. L., Quataert E., 2008, MNRAS, 390, 781
Michałowski M. J. et al., 2009, ApJ, 693, 347
Nakajima H., Shimokawabe T., Mori Y. A., Kudou Y., Kawai N., 2008, GCN, 8202, 1
Narayan R., Paczynski B., Piran T., 1992, ApJ, 395, L83
Norris J. P., Bonnell J. T., 2006, ApJ, 643, 266
Nysewander M., Fruchter A. S., Pe'er A., 2009, ApJ, 701, 824
Ofek E. O. et al., 2007, ApJ, 662, 1129
Pagani C., Racusin J., 2008, GCN, 8185, 1
Peng C. Y., Ho L. C., Impey C. D., Rix H.-W., 2002, AJ, 124, 266
Perley D. A. et al., 2009, ApJ, 696, 1871
Pettini M., Pagel B. E. J., 2004, MNRAS, 348, L59
Poggianti B. M., Barbaro G., 1997, A&A, 325, 1025
Prochaska J. X. et al., 2006, ApJ, 642, 989
Rieke G. H., Lebofsky M. J., 1985, ApJ, 288, 618
Rolleston W. R. J., Smartt S. J., Dufton P. L., Ryans R. S. I., 2000, A&A, 363, 537
Schlegel D. J., Finkbeiner D. P., Davis M., 1998, ApJ, 500, 525
Smartt S. J., Rolleston W. R. J., 1997, ApJ, 481, L47
Soderberg A. M. et al., 2006, ApJ, 650, 261
Stratta G. et al., 2007, A&A, 474, 827
Svensson K. M., Levan A. J., Tanvir N. R., Fruchter A. S., Strolger L., 2010, MNRAS, 405, 57
Tanvir N. R., Chapman R., Levan A. J., Priddey R. S., 2005, Nat, 438, 991
Thöne C. C. et al., 2008, ApJ, 676, 1151
Thronson H. A. Jr, Greenhouse M. A., 1988, ApJ, 327, 671
Tristram P., Castro-Tirado A. J., Yock P., Gorosabel J., de Ugarte Postigo A., 2008, GCN, 8181, 1
Troja E., King A. R., O 'Brien P. T., Lyons N., Cusumano G., 2008, MNRAS, 385, L10
Ukwatta T. N. et al., 2010, ApJ, 711, 1073
van Paradijs J. et al., 1997, Nat, 386, 686
Wainwright C., Berger E., Penprase B. E., 2007, ApJ, 657, 367
Wang C., Lai D., Han J. L., 2006, ApJ, 639, 1007
Wiersema K. et al., 2007, A&A, 464, 529
Woosley S. E., Bloom J. S., 2006, ARA&A, 44, 507
Xu D. et al., 2009, ApJ, 696, 971
Yi T., Liang E., Qin Y., Lu R., 2006, MNRAS, 367, 1751
Zhang B., Zhang B.-B., Liang E.-W., Gehrels N., Burrows D. N., Mészáros P., 2007, ApJ, 655, L25
Zhang B. et al., 2009, ApJ, 703, 1696

This paper has been typeset from a TEX/LATEX file prepared by the author.